

# Scaling Theory of the Mechanical Properties of Amorphous Nano-Films

Awadhesh K. Dubey<sup>1</sup>, H. George E. Hentschel<sup>2</sup>, Prabhat K. Jaiswal<sup>1</sup>,

Chandana Mondal<sup>1</sup>, Yoav G. Pollack<sup>1</sup>, and Itamar Procaccia<sup>1</sup>

<sup>1</sup>*Department of Chemical Physics, The Weizmann Institute of Science, Rehovot 76100, Israel*

<sup>2</sup>*Department of Physics, Emory University, Atlanta, Georgia*

Numerical Simulations are employed to create amorphous nano-films of a chosen thickness on a crystalline substrate which induces strain on the film. The films are grown by a vapor deposition technique which was recently developed to create very stable glassy films. Using the exact relations between the Hessian matrix and the shear and bulk moduli we explore the mechanical properties of the nano-films as a function of the density of the substrate and the film thickness. The existence of the substrate dominates the mechanical properties of the combined substrate-film system. Scaling concepts are then employed to achieve data collapse in a wide range of densities and film thicknesses.

Numerical simulations are notorious for their innate inability to explore large systems of experimental relevance. This shortcoming can be turned into an advantage in the study of nano-systems, providing a precious system-size dependence of the explored properties. Indeed, nanometer-thick films with designed compositions and microstructures occupy a central position in nano-materials research.

Thin films are everywhere around us and we are very much dependent on them in our everyday life. Thin films find huge applications in science and technology and their importance keeps on growing for a wide range of applicabilities [1–4] in areas such as electronic semiconductor devices, LEDs, optical coatings, hard coatings on cutting tools, for both energy, generation, e.g., thin film solar cells and storage. Amorphous thin films composed of rare-earth transition metals are heavily used for producing magnetic data storage devices [5, 6].

Though there have been plenty of experimental studies on both crystalline and amorphous thin films, there are very few theoretical and simulation studies [7, 8]. In particular a systematic investigation of the film-thickness and substrate density dependence of mechanical properties of amorphous thin films is still lacking despite their obvious technological importance. In most of the studies the main focus is bestowed upon the electronic and magnetic properties [9–11]. However, it is equally important to investigate their mechanical properties as these devices must be reliable, they must have structural integrity, and they must retain that integrity over their lifetime, mechanical failures must not occur.

In this Letter we explore how numerical simulations can shed new light on the mechanical properties of amorphous films grown on crystalline substrates. The central point of this Letter will be that using scaling concepts one can provide a predictive theory for the changes in the mechanical properties when the density of the substrate and the thickness of the film vary.

We will limit our study in this paper to the mechanical properties of thin films on substrates as the substrate

plays a key role in the properties of thin films. The substrate can induce huge stresses [12–14] on the film the nature of which depends on various factors such as the geometry of the substrate, lattice mismatch and difference in thermal expansion coefficients of the film and substrate etc.

The model discussed in the Letter grows a film of a binary glass on top of a crystalline substrate. The binary glass film is made from 65% particles A and 35% particles B, interacting via Lennard Jones (LJ) potentials with parameters  $\lambda_{BB}/\lambda_{AA} = 0.88$ ,  $\lambda_{AB}/\lambda_{AA} = 0.8$ ,  $\epsilon_{BB}/\epsilon_{AA} = 0.5$  and  $\epsilon_{AB}/\epsilon_{AA} = 1.5$ . This system has been extensively studied as a model glass former [15–17]. Lengths and energies are given in terms of  $\sigma_{AA}$  and  $\epsilon_{AA}$ , while time units are given by  $\sqrt{m\lambda_{AA}^2/\epsilon_{AA}}$ . Both the Boltzmann constant  $k_B$  and the mass of the particles are taken to be unity throughout. All the pair interactions are truncated at distance  $r_c$  where  $r_c/\lambda = 2.5$  with two continuous derivatives.

The films are grown in our simulations by a vapor deposition technique [18, 19] which closely mimics the physical vapor deposition technique in experiments where thin films are prepared by depositing hot molecules onto a substrate. In our simulations, we generated a crystalline substrate having four atomic layers along the  $z$  direction composed of  $N_S = 24 \times 28 \times 4$  particles interacting via Lennard-Jones with the characteristic size and energy:  $\lambda_{SS}/\lambda_{AA} = 0.8$ ,  $\lambda_{SA}/\lambda_{AA} = 0.8$ ,  $\lambda_{SB}/\lambda_{AA} = 0.8$ ,  $\epsilon_{SS}/\epsilon_{AA} = 1.5$ ,  $\epsilon_{SA}/\epsilon_{AA} = 1.5$  and  $\epsilon_{SB}/\epsilon_{AA} = 1.5$ . The substrate particles were organized in an hcp planar arrangement, with atoms restrained to their positions by a harmonic potential with spring constant  $K = 1000$ . The simulation box was kept periodic only in the  $x$  and  $y$  directions and the  $x$  and  $y$  box lengths are determined by the density  $\rho_S$  of the substrate. The volume of the system was kept constant, but the length of the simulation box in the  $z$  direction (perpendicular to the substrate) was sufficiently large to encompass a growing glass film and a vacuum region into which molecules were gradually introduced.

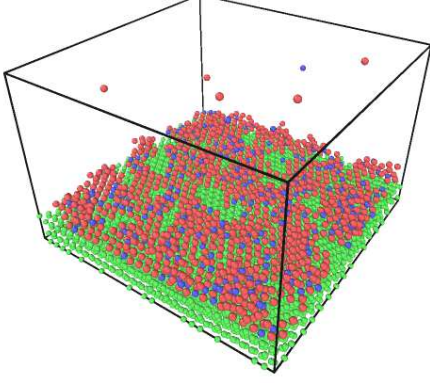


FIG. 1: Visualization of the process of deposition on the crystalline substrate of an amorphous film. In green are the substrate particles, and red and blue are particles A and B, respectively.

The actual algorithm consisted of depositions of a layer after layer of *A* and *B* particles, about 100 at a time, very close to the top of the free-surface. Each such deposition was followed by a procedure where the substrate and any previously deposited particles were maintained at the temperature  $T_S = 0.1$ , while simultaneously the newly added particles were first equilibrated at a hot temperature  $T_H = 0.7$ , then cooled down to  $T_S$  at a rate of  $3.33 \times 10^{-2}$ , and lastly equilibrated at  $T_S$  through the use of two Nosé-Hoover chains [18, 19] thermostat. We choose  $T_S = 0.1$  such that it is well below the reported glass transition temperature ( $T_g$ ) of the Kob-Anderson 65 : 35 binary mixture in 3D [20]. The process of deposition on top of the substrate is visualized in Fig 1.

After a prescribed number of particles have been deposited, depositions stopped and measurements are carried out after simulating the whole system at  $T_s$  for 120000 time units in steps of  $\delta t = 0.01$ . Measurements were performed 100 times for a total period of 2000 time units. We define two variables, the deposited film thickness  $w_D$  (according to substrate configuration) and the actual film thickness  $w$ . The number of particles to be deposited is determined, at the beginning of a simulation, by the formula  $N_D = Lx \times Ly \times w_D \times 1.2$ , where  $w_D$  is varied from 0.5 to 10.0. However, after deposition the top surface is not smooth and  $w$  is calculated by dividing the  $xy$ -area in small blocks and calculating the local height and averaging it over the blocks.

Having constructed the film of desired thickness over the substrate, we can compute its mechanical properties. Thus for example the shear modulus  $\mu_{xy}$  is obtained ex-

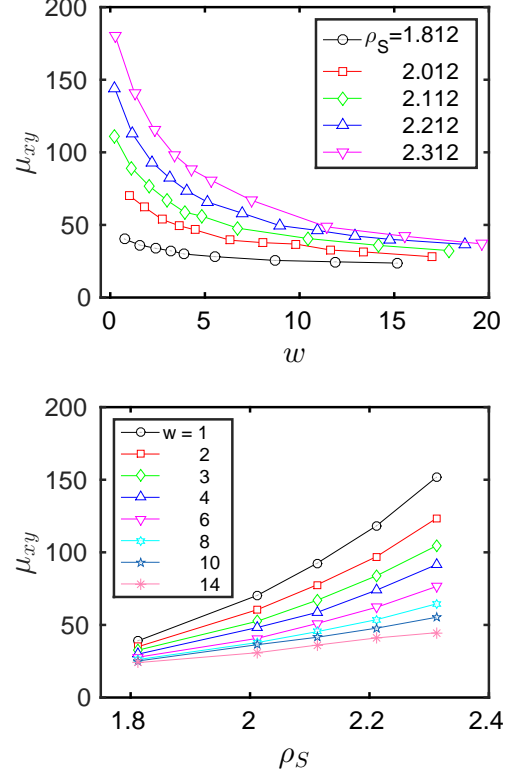


FIG. 2: Upper panel: the  $xy$  shear modulus as a function of film width for different values of the substrate density. Lower panel: the same modulus as a function of substrate density for different film widths.

actly as

$$\mu_{xy} = \mu_{xy}^B - \frac{V}{T} [\langle \sigma_{xy}^2 \rangle - \langle \sigma_{xy} \rangle^2], \quad (1)$$

where  $\sigma_{xy}$  is the  $xy$  component of the fluctuating stress tensor [21] and  $\mu_{xy}^B$  is the Born term [22] which has the explicit form

$$\begin{aligned} \mu_{xy}^B = & \frac{1}{V} \sum_{j>i} \left[ y_{ij}^2 \frac{1}{r_{ij}} \frac{\partial U}{\partial r_{ij}} + x_{ij}^2 y_{ij}^2 \left( \frac{1}{r_{ij}^2} \frac{\partial^2 U}{\partial r_{ij}^2} - \frac{1}{r_{ij}^3} \frac{\partial U}{\partial r_{ij}} \right) \right] \\ & + K \sum_{i=1}^{N_s} (y_i - y_{i_0})^2, \end{aligned} \quad (2)$$

where  $y_{i_0}$  is the reference  $y$ -coordinate of the  $i^{th}$  substrate-particle. The molecular dynamics code can be used now to measure the fluctuation in the stress tensor as well as the fluctuating inter-particle distances  $r_{ij}$ . Using this information both terms in the shear modulus can be computed. The computation is repeated twenty times and the shear modulus is averaged over these twenty runs. The results are shown in Fig. 2 as a function of the film

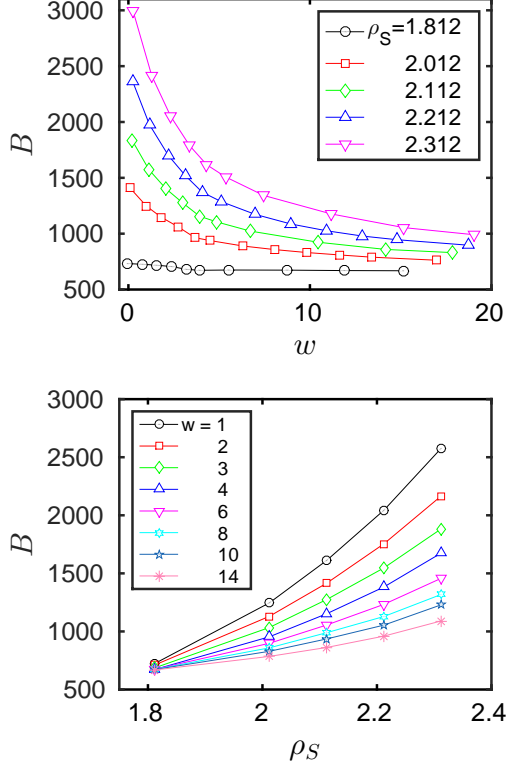


FIG. 3: Upper panel: the bulk modulus as a function of film width for different values of the substrate density. Lower panel: the same modulus as a function of substrate density for different film widths.

width  $w$  and of the substrate density  $\rho_S$ . Note the dramatic effect of the substrate density on the shear modulus, changing it (for small film width) by a factor of four when the substrate density changes by 25%. Clearly, this strong effect disappears upon increasing the film thickness and asymptotically the shear modulus converges to the bulk limit.

Similarly to the shear modulus the bulk modulus is given by the exact expression

$$B = B^B - \frac{V}{T}[\langle P^2 \rangle - \langle P \rangle^2], \quad (3)$$

where  $P$  is the fluctuating pressure and  $B^B$  is the Born term which has the explicit form

$$\begin{aligned} B^B &= \frac{1}{V} \sum_{j>i} \left[ (x_{ij}^2 + y_{ij}^2 + z_{ij}^2) \frac{1}{r_{ij}} \frac{\partial U}{\partial r_{ij}} \right. \\ &\quad \left. + (x_{ij}^2 + y_{ij}^2 + z_{ij}^2)^2 \left( \frac{1}{r_{ij}^2} \frac{\partial^2 U}{\partial r_{ij}^2} - \frac{1}{r_{ij}^3} \frac{\partial U}{\partial r_{ij}} \right) \right] \\ &\quad + K \sum_{i=1}^{N_S} [(x_i - x_{i_0})^2 + (y_i - y_{i_0})^2 + (z_i - z_{i_0})^2] (4) \end{aligned}$$

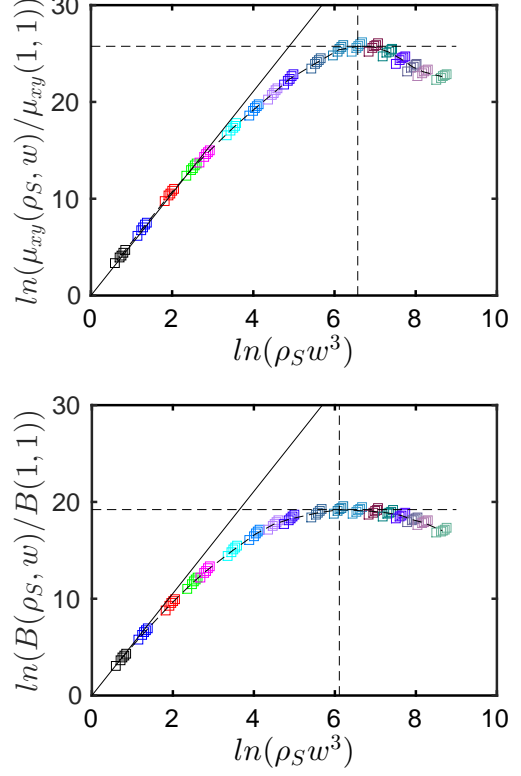


FIG. 4: The data collapse for the shear modulus (upper panel) and for the bulk modulus (lower panel).

Here,  $x_{i_0}$  and  $z_{i_0}$  are the reference  $x$ - and  $z$ -coordinates of the  $i^{th}$  substrate-particle. Both terms are readily computed in the MD code, and the average computed from twenty independent runs are shown in Fig. 3.

The effect of the substrate is as dramatic for the bulk modulus as for the shear modulus. Our next task is to understand these results and turn them into a predictive theory. Both the shear and the bulk moduli are functions of two variables, i.e.,  $\rho_S$  and  $w$ . It is advantageous to represent both objects as a function of a dimensionless variable, i.e.,  $x = \rho_S w^3$ . Needless to say, we need to preserve dimensions, so we try a representation in the form

$$\mu_{xy}(\rho_S, w) = \mu_{xy}(1, 1) f_\mu(\rho_S w^3), \quad (5)$$

$$B(\rho_S, w) = B(1, 1) f_B(\rho_S w^3). \quad (6)$$

The form of the scaling functions  $f_\mu$  and  $f_B$  can be gleaned from the data collapse shown in Fig. 4. The almost perfect data collapse begs the next questions: (i) what is the slope of the functions  $f_\mu(x)$  and  $f_B(x)$  in the limit  $x \rightarrow 1$  and (ii) what determines the position of the maximum of these two functions. Obviously, these must be determined by the parameters of the model.

To understand the slope we examine the potential of

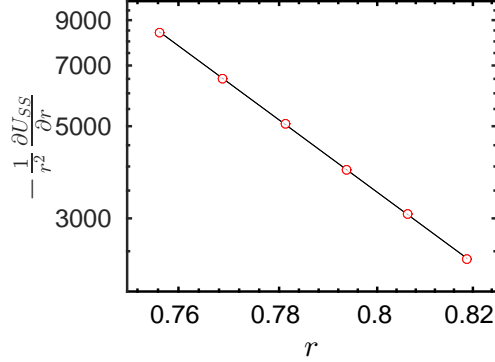


FIG. 5: The effective power law in the range of scales determined by the range of substrate densities  $r_0/\lambda \in [\rho_{S,max}^{-1/3}, \rho_{S,min}^{-1/3}]$ .

interaction between the substrate particles. This interaction defines a typical scale

$$r_0 \sim \frac{\lambda_{SS}}{\rho_S^{1/3}}. \quad (7)$$

In Fig. 5 we demonstrate that in the range of substrate densities considered here the interaction is represented to a very good approximation as an effective power law [23]

$$-\frac{1}{r^2} \frac{\partial U_{SS}(r)}{\partial r} \sim \frac{\epsilon_{SS}}{\lambda_{SS}^3} \left( \frac{r}{\lambda_{SS}} \right)^{-3\nu}, \quad (8)$$

which serves as a definition of the effective exponent  $\nu$  which in our case takes on the value  $\nu = 5.27$ . In the limit  $w \rightarrow 1$  the shear modulus is dominated by the substrate density, and from dimensional considerations we expect that [23]

$$\mu_{xy}(x \rightarrow 1) \sim \frac{\epsilon_{SS}}{\lambda_{SS}^3} \rho_S^\nu. \quad (9)$$

Indeed the initial slope in Fig. 4 agrees very well with this estimate. The argument is identical for the bulk modulus (the same dimensional considerations) and indeed the initial slopes are the same for both quantities. We thus end up with the prediction

$$f_\mu(x) \sim f_B(x) \sim x^\nu, \quad \text{for } x \ll x_c, \quad (10)$$

where  $\ln x_c$  is the point of maximum in Fig. 4. The other limit is obvious, reading as  $x \rightarrow \infty$

$$f_\mu(x) \rightarrow \frac{\mu_{xy}^\infty}{\mu_{xy}(1,1)}, \quad f_B(x) \rightarrow \frac{B^\infty}{B(1,1)}. \quad (11)$$

where  $\mu_{xy}^\infty$  and  $B^\infty$  are the shear and bulk moduli for the pure glassy phase. Finally we need to understand the

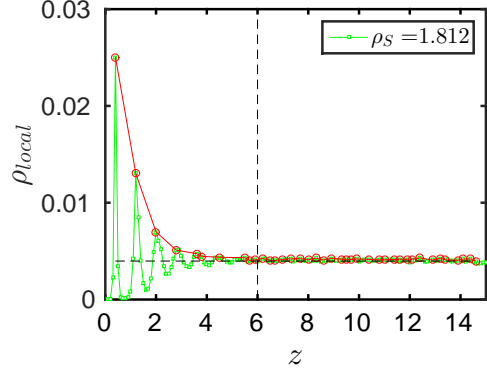


FIG. 6: The local density of the glassy film as a function of the  $z$ -coordinate (green). The influence length of the substrate is estimated from here to be  $\xi_S \approx 6$ . The envelope of the data is shown in red color.

point of maximum  $\ln x_c$ . This must be determined by the typical scale, say  $\xi_S$ , characterizing the influence of the substrate on the properties of the film. This length can be read straightforwardly from the local density of the film as a function of the coordinate  $z$ . A typical such plot is shown in Fig. 6, from which we can estimate  $\xi_S \approx 6$ . Since  $\rho_S \approx 2$ , we can estimate  $\ln x_c \approx \ln(\rho_S \xi_S^3) \approx 6$  as seen indeed in Fig. 4.

Having at hand scaling functions one can predict the values of the shear and bulk moduli for any value of  $w$  or  $\rho_S$  where these properties are not measured. Moreover, any quantity with the same dimensions is expected to have a scaling function having the same initial slope and a maximum at the same value of  $w^3 \rho_S$ . Other mechanical properties like the Young modulus and the Poisson ratio also succumb to scaling concepts, but the presentation of that theory is beyond the scope of the present Letter and will be expounded in a forthcoming publication.

This work had been supported in part by an “ideas” grant STANPAS of the European Research Council (ERC) and by the Minerva Foundation, Munich, Germany. We acknowledge with thanks fruitful discussions with Shiladitya Sengupta and Murari Singh. PKJ acknowledges VATAT fellowship from the Council of Higher Education, Israel.

- 
- [1] A.A.R. Elshabini-Riad and F.D. Barlow, *Thin Film Technology Handbook*, New York: McGraw-Hill (1997).
  - [2] R. Ramirez-Bon and F.J. Espinoza-Beltrán (eds.), *Deposition, Characterization and Applications of Semiconductor Thin Films*, Research Signpost (2009).
  - [3] S. Reineke, *Rev. Mod. Phys.* **85**, 1245 (2013).
  - [4] I. Moreno and J.J. Araiza, *Optics Letters* **30**, 914 (2005).

- [5] J.C. Lodder, MRS Bull. **20**, 59 (1995).
- [6] J.L. Simonds, Phys. Today **48**, 26 (1995).
- [7] C. Dong, S. Chen, T.Y. Hsu (Xu Zuyao), Journal of Magnetism and Magnetic Materials **250**, 288 (2002).
- [8] C. J. Robinson, M. G. Samant, and E. E. Marinero, Appl. Phys. A **49**, 619 (1989).
- [9] H.J. Leamy and A.G. Dirks, J. Appl. Phys. **49**, 3430 (1978).
- [10] J.W. Lee, B.G. Demczyk, K.R. Mountfield and D.E. Laughlin, J. Appl. Phys. **63**, 2905 (1988).
- [11] A.T. Hindmarch, A.W. Rushforth, R.P. Champion, C.H. Marrows, and B.L. Gallagher, Phys. Rev. B **83**, 212404 (2011).
- [12] K. Mandal, M. VaHzquez, D. GarcmHa, F.J. Castano, C. Prados, A. Hernando, Journal of Magnetism and Magnetic Materials **220**, 152 (2000).
- [13] K. Mandal, Physics Letters A **174**, 151 (1993).
- [14] F. Ernenge and H. Kronmull, Phys. Stat. Sol. A **80**, 195 (1983).
- [15] W. Kob and H.C. Andersen, Phys. Rev. E, **51**, 4626 (1995).
- [16] K. Vollmayr, W. Kob, and K. Binder, J. Chem. Phys. **105**, 4714 (1996).
- [17] S. Sastry, P.G. Debenedetti, and F.H. Stillinger, Nature (London) **393**, 554 (1998).
- [18] S. Singh and J.J. de Pablo, J. Chem. Phys. **134**, 194903 (2011).
- [19] R. Gutiérrez, S. Karmakar, Y.G. Pollack, and I. Procaccia, Euro. Phys. Lett., **111**, 56009 (2015) .
- [20] P. Crowther, F. Turci, C.P. Royall, J. Chem. Phys. **143**, 044503 (2015).
- [21] J.P. Wittmer, H. Xu, P. Políńska, F. Weysser, and J. Baschnagel, J. Chem. Phys. **138**, 12A533 (2013).
- [22] H.G.E. Hentschel, S. Karmakar, E. Lerner, and I. Procaccia, Phys. Rev. E **83**, 061101 (2011).
- [23] E. Lerner and I. Procaccia, Phys. Rev. E **80**, 026128 (2009).